

# RSC Advances



This is an *Accepted Manuscript*, which has been through the Royal Society of Chemistry peer review process and has been accepted for publication.

*Accepted Manuscripts* are published online shortly after acceptance, before technical editing, formatting and proof reading. Using this free service, authors can make their results available to the community, in citable form, before we publish the edited article. This *Accepted Manuscript* will be replaced by the edited, formatted and paginated article as soon as this is available.

You can find more information about *Accepted Manuscripts* in the [Information for Authors](#).

Please note that technical editing may introduce minor changes to the text and/or graphics, which may alter content. The journal's standard [Terms & Conditions](#) and the [Ethical guidelines](#) still apply. In no event shall the Royal Society of Chemistry be held responsible for any errors or omissions in this *Accepted Manuscript* or any consequences arising from the use of any information it contains.



Journal Name

COMMUNICATION

## Hierarchical self-assembly of random mica nanosheet-stabilized silver nanoparticles into flower microstructures for highly sensitive SERS substrates

Received 00th January 20xx,  
Accepted 00th January 20xx

DOI: 10.1039/x0xx00000x

www.rsc.org/

Chih-Wei Chiu\* and Po-Hsien Lin

In this study, we observed the formation of flower-like microstructures by the hierarchical self-assembly of random mica nanosheet (RMN)-stabilized silver nanoparticles (AgNPs) without organic stabilizers. The SERS spectra of adenine molecules from DNA were measured as functions of the AgNP sizes and microstructures with substrates formed using various RMN/AgNP precursor ratios. The AgNP@RMN substrates significantly contributed to the high SERS sensitivity to adenine molecules with an SERS enhancement factor (EF) of  $1.5 \times 10^5$ . These novel AgNP@RMN hybrid microstructures can be utilized as SERS substrates for biological sensing applications.

### Introduction

In recent years, the study of nano-manipulating technologies has enabled the self-assembly of molecular units into highly ordered structures.<sup>1</sup> Self-assembly is a promising bottom-up process for the fabrication of next-generation nanomaterials, which have been shown to exhibit unique physical and chemical properties compared to bulk analogs.<sup>2,3</sup> Synthetic self-assembled nanomaterials with different shapes, such as cubes,<sup>4</sup> spheres,<sup>5</sup> wires,<sup>6</sup> tubes,<sup>7</sup> fibers,<sup>8</sup> rings,<sup>9</sup> discs,<sup>10</sup> and flowers,<sup>11</sup> have been extensively reported recently. Such bottom-up syntheses are typically driven by non-covalent bonding forces, such as ionic charge interactions, dipole-dipole forces, hydrogen bonding, van der Waals forces,  $\pi$ - $\pi$  stacking, and hydrophobic interactions.<sup>12–14</sup>

The synthesis of nanoparticles (NPs) with controlled sizes and shapes is an important research issue. Common organic surfactants and amphiphilic polymers are frequently employed for stabilizing the generated NPs. The presence of organic surfactants provides templates for tailoring silver NP (AgNP)

shapes into spherical, triangular, and fibrous morphologies.<sup>15</sup> AgNPs are of particular research interest because they possess unique properties for conduction,<sup>16</sup> catalysis,<sup>17</sup> biosensing,<sup>18</sup> and as additives in composite fibers.<sup>19</sup> Recent developments in electronic devices include the decrease in thickness of conductive films and the width of printed circuits, requiring the synthesis of AgNPs in different forms such as conductive pastes.<sup>20</sup> The catalytic activity of AgNPs has been found to depend on the particle size distribution,<sup>21</sup> structure,<sup>22</sup> shape,<sup>23</sup> and support.<sup>24</sup>

Surface-enhanced Raman spectroscopy (SERS) is a newly developed spectroscopic technique based on the signal enhancement of Raman scattering via chemical effects and localized surface plasmon resonance.<sup>25–28</sup> Powerful signals from molecules attached to Ag or Au NPs can provide high-sensitivity structural information on the molecules; the non-destructive detection of single molecules is possible by this method. The technique has been demonstrated in large-scale bio-sensing applications, exhibiting the rapid detection of molecules from DNA, viruses, bacteria, and cells.<sup>29–31</sup>

Previously, we demonstrated an exfoliation process that allowed the randomization of a smectite Na<sup>+</sup>-mica layered structure using polyamine quaternary salts; the randomized mica nanosheets (RMN) were subsequently isolated in an aqueous suspension.<sup>32</sup> The random platelets had a surface area of 720 m<sup>2</sup>/g and ~18,000 ionic charges per platelet. We additionally reported the self-assembly of RMN into ordered arrays with dendrite-, cubic-, rod-, and fiber-like microstructures.<sup>33</sup>

In this study, inorganic plate-like mica clays were used to support the formation of colloidal AgNPs in the absence of organic stabilizers. Without the contamination of organic surfactants, the generated AgNPs and RMN nanohybrids (AgNP@RMN) could self-assemble into substrates with various morphologies, such as rod- and flower-like microstructures, by controlling the weight fraction of AgNPs on the nanosheets. These observations were made using field-emission scanning electronic microscopy (FE-SEM) micrographs. The flower-like hybrid microstructures were tested as SERS substrates, and

Department of Materials Science and Engineering, National Taiwan University of Science and Technology, Taipei 10607, Taiwan

\*Corresponding author: Tel: +886-2-2737-6521; Fax: +886-2-2737-6544; E-mail: cwchiu@mail.ntust.edu.tw

Electronic Supplementary Information (ESI) available: [FE-SEM micrographs and XRD analysis of RMN/AgNP nanohybrids are available in the supporting information]. See DOI: 10.1039/x0xx00000x

were shown to allow the highly efficient detection of adenine molecules from DNA. While the design of SERS substrates using only AgNPs remains problematic, the AgNP@RMN hybrid design exhibited greater stability than monometallic AgNPs. This stability may overcome certain difficulties, such as the sensitivity of Ag to oxidation in air. Therefore, this new class of SERS substrates based on AgNP@RMN flower-like microstructures could be applied in biomedical devices.

## Experimental

### Materials

The synthetic fluorinated Na<sup>+</sup>-mica clay (mica, SOMASIF ME-100, CO-OP Chemical Co., Japan) used in this study had a layered silicate structure composed of 26.5 wt% Si, 15.6 wt% Mg, 0.2 wt%, 8.8 wt% F, 4.1 wt% Na, and 0.1 wt% Fe with the balance being O. The mica had a layered structure of 2:1 silicate/aluminum oxide, with two tetrahedral sheets sandwiching an edge-shared octahedral sheet. The aluminosilicate mica had exchangeable Na<sup>+</sup> counter-ions with a cationic exchange capacity (CEC) of 120 meq/100 g. AgNO<sub>3</sub> (purity 99.9%) was purchased from Aldrich Chemical Co. Ethanol (purity >99.5%, SHOWA) was additionally utilized as a reducing agent for AgNO<sub>3</sub>. Adenine powder (purity 99.9%) was purchased from Sigma-Aldrich.

### One-step exfoliation of layered mica into RMN in water suspension

The one-step exfoliation of the Na<sup>+</sup>-mica clay to prepare delaminated mica nanosheets using poly(oxypropylene)-amine-salt has been previously reported.<sup>32,33</sup> The exfoliated sheets were dispersed in water and purified by a solvent-extraction process. The RMN were characterized as featureless using X-ray powder diffraction (XRD) and zeta potential analysis to determine the surface ionic character. The ionic RMN were hydrophilic, dispersible in water, and estimated at approximately 300–1000 nm in diameter and 1 nm in thickness via atomic force microscopy (AFM) and transmission electron microscopy (TEM).

### Synthesis of AgNPs in the presence of RMN

An RMN slurry (0.04 g of RMN in 4 g ethanol; 1 wt%) was first prepared by agitation and soaking the RMN in ethanol at 25 °C for 30 min, followed by the addition of 1 wt% AgNO<sub>3</sub> solution in deionized water at the designed weight ratios of RMN/AgNO<sub>3</sub> of 1:0, 10:1, 5:1, and 1:1. The mixture was stirred vigorously at 300–600 rpm and 60 °C for 12 h. The reaction progress was monitored by observing the color change from yellow to dark yellow, indicating the reduction of Ag<sup>+</sup> to Ag<sup>0</sup>. The UV absorption was measured at the sample concentration of 0.1 g product in 3.0 g distilled water. The products were further analyzed by TEM.

### Self-assembly of AgNP@RMN hybrids into microstructured SERS substrates

The AgNP@RMN hybrid suspensions were dispersed in co-solvents of water and ethanol at a concentration of 1 wt%. The resulting solution was drop-coated on a 2 cm × 2 cm clean glass substrate and then evaporated in an oven at 80 °C for 8 h

to form a thin film. The self-assembled morphologies in the dried film were monitored by FE-SEM, energy dispersive spectrometry (EDS), and XRD analyses.

### Preparation of SERS samples

In a typical synthesis, 2 μL adenine solution at various concentrations (1.0 × 10<sup>-2</sup> M, 1.0 × 10<sup>-3</sup> M, and 1.0 × 10<sup>-4</sup> M) was drop-coated onto the various AgNP@RMN hybrid substrates and dried under ambient conditions. The substrates were washed thoroughly with ethanol to remove unbound adenine molecules and then dried at room temperature to evaporate all ethanol. The final samples were then observed by Raman spectromicroscopy measurements.

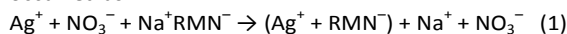
### Characterization and instruments

The AgNP solution was characterized by UV-vis absorption using a Shimadzu UV-2450 spectrophotometer. TEM was performed on a Zeiss EM 902A operated at 80 kV. The samples (1 wt% in deionized water) were deposited onto a C-coated Cu grid. FE-SEM was performed on a Zeiss EM 902A operated at 80 kV. The samples were prepared by dropping the AgNP@RMN suspension onto clean glass surfaces, followed by 8 h dehydration in an oven at 80 °C. The samples were then fixed onto a FE-SEM holder with conductive C paste and coated with a thin layer of Au prior to measuring. Surface element analysis was performed using EDS (OXFORD INCA ENERGY 400). The XRD (Schimadzu SD-D1 diffractometer) measurements were performed in a 2-theta scan configuration in the range of 20–90°. Raman scattering spectra were recorded with a ProMaker confocal Raman microscope system and integrated by the Protrustech Corp., Ltd, Taiwan. A laser operating at λ = 532 nm was used as the excitation source with a laser power of 20 mW and a 10-s exposure time. The laser line was focused onto the substrate in backscattering geometry using a 50× objective lens providing an excitation area of ~4 μm<sup>2</sup>.

## Results and discussion

### Synthesis of AgNPs by the associated RMN for converting AgNO<sub>3</sub> to AgNPs

The one-step exfoliation of the Na<sup>+</sup>-mica layered structure by polyamine into RMN resulted in a suspension of nanosheet platelets with high surface ionic charges of 18,000 ions/platelet and thin geometries of 300–1000 nm diameters and 1 nm thicknesses.<sup>32,33</sup> The uniform formation of AgNPs was stabilized through the ionic charge interactions between Ag<sup>+</sup> and RMN (Fig. 1a). The synthesis of AgNPs supported on RMN surfaces was performed using ethanol as a reducing agent.<sup>34</sup> The mechanism for reduction may have involved the binding of Ag<sup>+</sup> ions to RMN, which possessed oxygen ions and reduction functionality. The redox reaction with ethanol occurred as:



where (Ag<sup>+</sup> + RMN<sup>-</sup>) represents Ag<sup>+</sup> bound to the oxygen ions on the surface of RMN. The resulting Ag<sup>0</sup> species was free to migrate and aggregate into AgNPs, as follows:

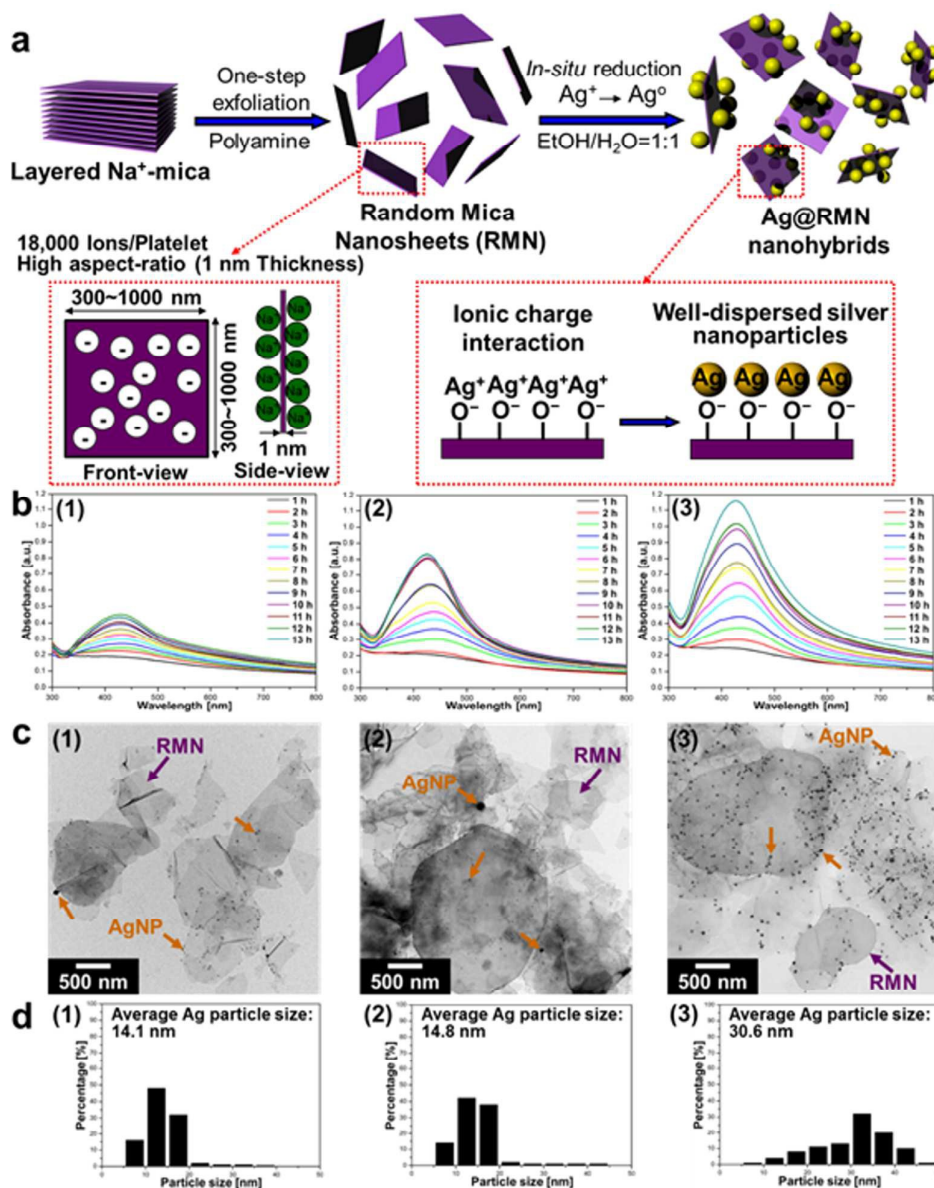
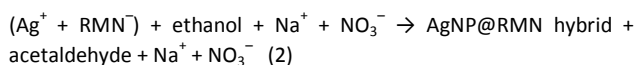


**Fig. 1** (a) Schematic of the one-step exfoliation of the  $\text{Na}^+$ -mica layered structure into random mica nanosheets (RMN) by the addition of polyamine salt and of the surface ionic charges on the resulting thin platelets. The AgNP@RMN hybrid is stabilized by ionic charge interactions. (b) UV-vis absorption spectra, (c) TEM micrographs, and (d) particle size histograms based on the TEM micrographs of colloidal AgNPs in a complex of RMN and  $\text{AgNO}_3$  at different precursor weight ratios of (1) 10:1, (2) 5:1, and (3) 1:1.



To identify the stabilization of AgNP@RMN, the synthesis of AgNPs was performed by mixing aqueous solutions of RMN and  $\text{AgNO}_3$  with 10:1, 5:1, and 1:1 weight ratios (henceforth referred to as the precursor weight ratios) at 60 °C (Fig. 1b, with results summarized in Table 1). Through the *in situ* reduction of  $\text{AgNO}_3$  to AgNPs in the presence of RMN as the stabilizer, the AgNP solution developed a golden-yellow color. The UV-vis spectra of the various solutions indicated the

presence of nanometer-scale Ag particles by the characteristic absorption peak at 420–430 nm after 12–13 h stirring. Through this reduction, ethanol effectively converted  $\text{AgNO}_3$  to stable AgNPs on the surface of RMN. The reduction of  $\text{Ag}^+$  formed  $\text{Ag}^0$  clusters that ultimately became AgNPs. The RMN, which possessed oxygen-ion-containing functional groups, first formed complexes with  $\text{Ag}^+$  and subsequently served as a stabilizer for the generated AgNPs. The presence of RMN effectively bound the Ag species and controlled the growth of  $\text{Ag}^0$  clusters.

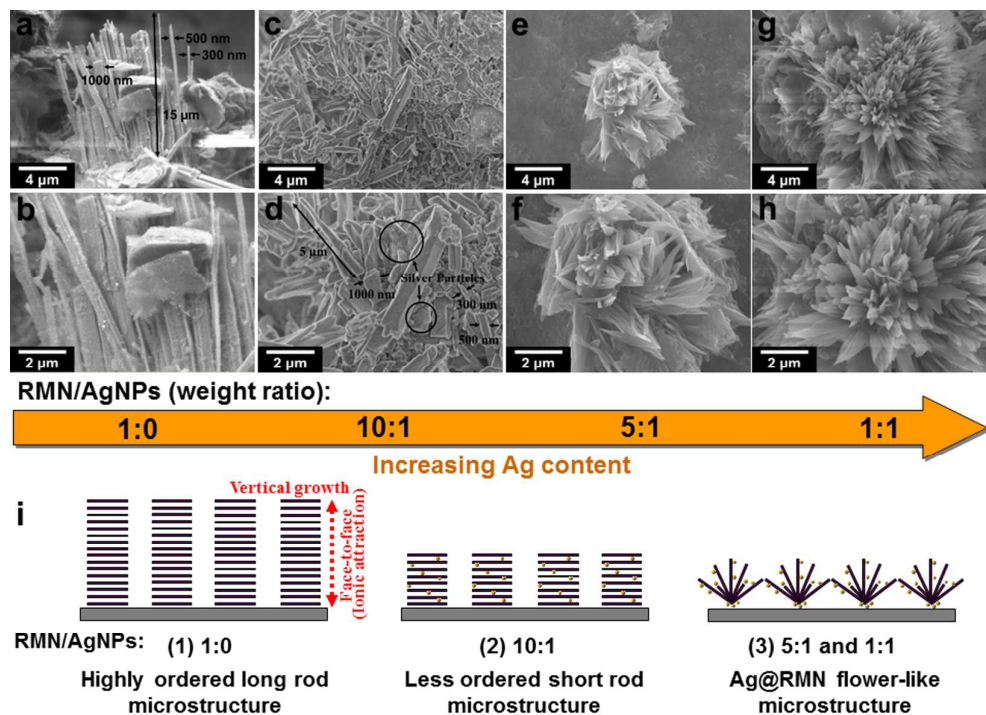
**Table 1.** UV-Vis absorption, Ag particle size, SERS EF values, and observations of self-assembly of the AgNP@RMN nano hybrids at different precursor weight ratios.

Sample	Weight ratio (w/w)	UV-Vis absorption (nm)	Average Ag particle size (nm) <sup>a</sup>	Observed self-assemblages by FE-SEM	SERS EF values <sup>b</sup>
RMN/AgNO <sub>3</sub>	1:0	--	--	Highly ordered long rod microstructure (10–15 μm in length and 300–1000 nm in width)	--
	10:1	426	14.1	Less-ordered short rod microstructure (1–5 μm in length and 300–1000 nm in width)	1.5 × 10 <sup>5</sup>
	5:1	427	14.8	Flower-like microstructure	4.8 × 10 <sup>4</sup>
	1:1	430	30.6	Flower-like microstructure	3.9 × 10 <sup>4</sup>
Na <sup>+</sup> -mica	--	--	--	--	--

<sup>a</sup> As measured by TEM.<sup>b</sup> The enhancement factor (EF) of SERS activity based on calculations by the equation  $EF = (I_{SERS}/C_{SERS})/(I_{ref}/C_{ref})$ .<sup>36–38</sup> In this equation,  $C_{ref}$  (1.0 M) and  $C_{SERS}$  represent the concentrations of adenine on the AgNP@RMN substrate, while  $I_{SERS}$  and  $I_{ref}$  represent the signal intensities obtained from adenine on AgNP@RMN and glass substrates, respectively.

The AgNP@RMN nano hybrids are finely dispersed in water as observed by TEM (Fig. 1c). The AgNPs on the RMN surface are observed to have particle diameters of ~15 nm, and are located on the RMN platelet rims. During the reduction reaction, AgNPs experience simultaneous nucleation and growth while adhered to the sheet surface. As summarized in Fig. 1d and Table 1, the average particle sizes and dispersity of the AgNPs depend on the relative amount of RMN. The

average size of the AgNPs clearly decreases from 30.6 to 14.1 nm, and the size distribution narrows as the ratio of mica sheets is increased. The different stabilities of the AgNP colloids on RMN are attributed to the strong interactions between the AgNPs and the RMN matrix. Therefore, the AgNP@RMN hybrid solution with a 10:1 precursor weight ratio shows the highest stability of dispersed AgNPs on the RMN surface.

**Fig. 2** FE-SEM micrographs at different magnifications of rod- and flower-like microstructures from the self-assembly of AgNP@RMN nano hybrids at different precursor weight ratios of (a and b) 1:0 (control), (c and d) 10:1, (e and f) 5:1, and (g and h) 1:1. (i) Conceptual illustration of the AgNP@RMN self-assembly routes of various microstructures with varied AgNP concentrations.

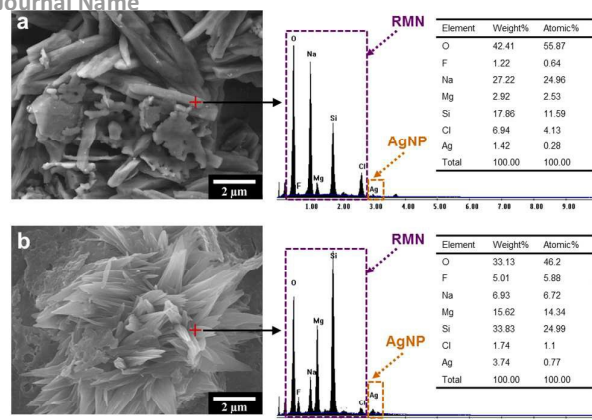


**Fig. 3** EDS analyses of the rod- and flower-like AgNP@RMN nanohybrid microstructures at precursor weight ratios of (a) 10:1 and (b) 5:1.

### Self-assembly into rod- and flower-like microstructures

Because of the high-aspect-ratio geometric shapes and intense ionic charges of the platelets, RMN has a tendency to self-assemble.<sup>33</sup> Mica sheets at 1 wt% in water were evaporated at 80 °C to produce powdered solids. The FE-SEM micrographs in **Fig. 2a** and **b** show the resulting rod-like microstructures, which have lengths of 10–15 μm and widths of 300–1000 nm, from the self-assembly of AgNP@RMN hybrids at the 1:0 precursor weight ratio. In control experiments, the pristine mica demonstrated amorphous or irregularly aggregated morphologies after the evaporation of water (see ESI **Fig. S1**). At the 10:1 precursor weight ratio, the AgNP@RMN hybrids self-align into short arrays with 1–5 μm lengths and 300–1000 nm widths (**Fig. 2c** and **d**). At 5:1 and 1:1 precursor ratios, the nanohybrids demonstrate self-assembled flower-like microstructures after water evaporation (**Fig. 2e–h** and **Fig. S2**).

The self-assembly mechanism for the rod-like microstructures results from face-to-face platelet piling through ionic charge attraction (**Fig. 2i**). Single mica sheets are self-piled into rod-like microstructures with lengths that depend on the precursor weight ratios. The observation of uniform rod-like structures shows that random sheets self-select for platelets with similar sizes within a given rod. When the precursor weight ratios are changed to 5:1 and 1:1, the formation of novel flower-like AgNP@RMN microstructures occurs, indicating that the strong stacking propensity triggers assembly with AgNPs acting as nucleating agents. The non-covalent interactions of AgNPs and RMN control the directional flower-like morphologies.

EDS analyses indicated element distributions of 42.41% O, 1.22% F, 27.22% Na, 2.92% Mg, 17.86% Si, 6.94% Cl, and 1.42% Ag for the rod-like AgNP@RMN microstructures at the 10:1 precursor weight ratio (**Fig. 3a**), and 33.13% O, 5.01% F, 6.93% Na, 15.62% Mg, 33.83% Si, 1.74% Cl, and 3.74% Ag for the flower-like AgNP@RMN microstructures at the 5:1 precursor weight ratio (**Fig. 3b**). The XRD patterns of the AgNP@RMN hybrids are shown in **Fig. S3** (see ESI). The AgNPs are crystalline, as the XRD patterns showed peaks at  $2\theta = 38^\circ, 44^\circ, 64^\circ,$  and  $77^\circ$ , which correspond to the (111), (200), (220), and (311) planes of fcc Ag, respectively. This confirms the presence of metallic Ag in the nanohybrids.

### Relationship between SERS intensities and AgNP@RMN hybrids

**Fig. 4** and **Table 1** show a series of SERS spectra of adenine molecules adsorbed onto different assembled AgNP@RMN substrates. The typical ring breathing mode resonance of adenine is indicated at the wavenumber of  $733\text{ cm}^{-1}$ ; additionally, bands are attributed to modes from the SERS measurements obtained in the previous study.<sup>35</sup> The AgNP@RMN hybrid SERS substrates were produced from

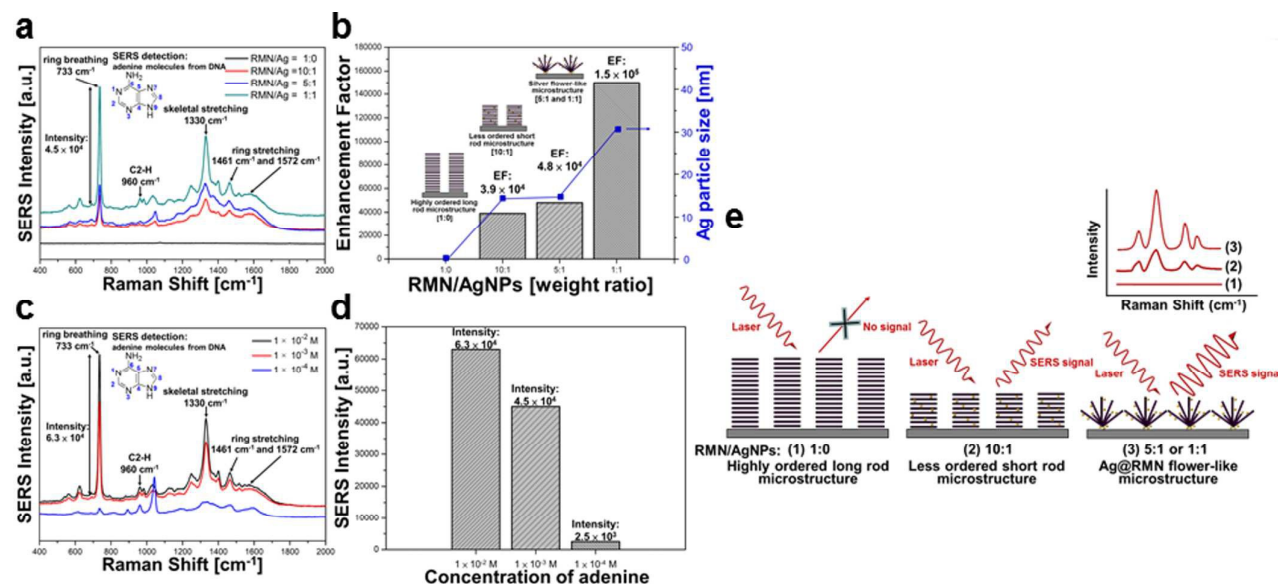


**Fig. 4** The relationship between SERS signal intensity and AgNP particle size AgNPs using adenine molecules. (a) SERS spectra of  $1.0 \times 10^{-3}$  M adenine molecules adsorbed on AgNP@RMN hybrid substrates at the wavenumber of  $733\text{ cm}^{-1}$ , measured using substrates with various precursor weight ratios. (b) SERS EF values of adenine as a function of the particle size and microstructure. (c) SERS spectra of various concentrations of adenine solutions on AgNP@RMN with a 1:1 precursor weight ratio. (d) Signal intensity of adenine as a function of the adenine solution concentration. (e) Schematic of the AgNP@RMN hybrid SERS substrate interacting with adenine molecules. (A laser operating at  $\lambda = 532\text{ nm}$  was used as the excitation source at 20 mW power. All Raman spectra were obtained with 10 s exposure time.)

drop-coating the hybrid suspensions onto glass, followed by evaporating the aqueous solvent at 80 °C to form thin films. Adenine solutions of  $1.0 \times 10^{-2}$  M,  $1.0 \times 10^{-3}$  M, and  $1.0 \times 10^{-4}$  M were drop-coated onto the synthesized SERS substrates. The relationship between the SERS spectra and enhancement factor (EF) values for the adenine molecules and AgNP@RMN hybrids is illustrated in Fig. 4a and b. No significant signal appears in the SERS spectrum in the absence of the rod-like AgNP@RMN nanohybrids formed at the 1:0 precursor weight ratio. As the Ag loading is increased, Raman bands at  $733 \text{ cm}^{-1}$  occur that correspond to adenine molecules. When the precursor weight ratio of the AgNP@RMN is 1:1, the SERS signal attains the EF value of  $1.5 \times 10^5$ . Fig. 4c and d show a series of SERS spectra from adenine molecules adsorbed on the AgNP@RMN substrates with different adenine concentrations. As the adenine concentration and Ag loading on the substrate increase, both the areal density of AgNPs and the number density of adenine molecules adsorbed per unit area of the nanohybrid substrate increase. In these spectra, the intensities of the Raman peaks correspondingly increase. This demonstrates the production of a novel SERS substrate with a highly significant sensitivity to adenine by immobilizing AgNPs on the double-edged sides of nanometers-thick mica sheets (Fig. 4e). The AgNP@RMN nanohybrids produced SERS substrates that allowed the highly efficient detection of adenine molecules because of the arrangement of AgNP@RMN in the high-surface-area flower-like microstructures. A significant SERS signal enhancement was observed in the bio-detection of adenine molecules from DNA. The novel morphologies of the AgNP@RMN SERS bio-devices could be extended to applications with microorganisms and larger biological units, such as fungi and cancer cells.

## Conclusions

We fabricated SERS substrates using hierarchical self-assembled flower-like microstructures of AgNPs on RMN templates. The homogenous AgNP@RMN hybrids were synthesized by the *in situ* reduction of  $\text{AgNO}_3$  using ethanol as a reducing agent. The narrow size distribution of spherical  $\sim 15$  nm AgNPs on the rim of the RMN sheets resulted from the inherent uneven charge distribution over the RMN platelets. After the fine dispersion of AgNP@RMN in water and the controlled evaporation of the solvent, the AgNPs acted as nucleating agents to change the morphology of the rods into flower-like microstructures. The shape and high surface area of these hierarchical AgNP@RMN microstructures exhibited excellent SERS enhancement abilities. When the precursor weight ratio of AgNP@RMN was 1:1, the observed Raman bands in the SERS signal were attributed to adenine molecules at the wavenumber of  $733 \text{ cm}^{-1}$ . The signal was observed with the highly significant EF value of  $1.5 \times 10^5$ . The flower-like AgNP@RMN microstructures could have potential applications in anti-bacterial sensors, catalysts, and gas sensors.

## Acknowledgments

We acknowledge financial support from the Aim for the Top University Plan of the National Taiwan University of Science and Technology and the Ministry of Science and Technology (MOST 103-2221-E-011-167- and MOST 104-2221-E-011-155-) of Taiwan.

## Notes and references

- H. Qiu, Z. M. Hudson, M. A. Winnik and I. Manners, *Science*, 2015, **347**, 1329–1332.
- A. K. Sundramoorthy, Y. Wang, J. Wang, J. Che, Y. X. Thong, A. C. W. Lu and M. B. Chan-Park, *Sci. Rep.*, 2015, **5**, 10716.
- C. W. Chiu, C. A. Lin and P. D. Hong, *J. Polym. Res.*, 2011, **18**, 367–372.
- J. Chen, J. Mao, J. Zhao, M. Ren and M. Wei, *RSC Adv.*, 2014, **4**, 28832–28835.
- J. Gopal, M. Manikandan and H. F. Wu, *RSC Adv.*, 2014, **4**, 10982–10989.
- C. M. Fu, K. S. Jeng, Y. H. Li, Y. C. Hsu, M. H. Chi, W. B. Jian and J. T. Chen, *Macromol. Chem. Phys.*, 2015, **216**, 59–68.
- J. Wu, H. Xu and W. Yan, *RSC Adv.*, 2015, **5**, 19284–19293.
- Z. Liang, G. Zheng, C. Liu, N. Liu, W. Li, K. Yan, H. Yao, P. C. Hsu, S. Chu and Y. Cui, *Nano Lett.*, 2015, **15**, 2910–2916.
- H. Yamagishi, T. Fukino, D. Hashizume, T. Mori, Y. Inoue, T. Hikima, M. Takata and T. Aida, *J. Am. Chem. Soc.*, 2015, **137**, 7628–7631.
- M. H. Chi, Y. H. Kao, T. H. Wei, C. W. Lee and J. T. Chen, *Nanoscale*, 2014, **6**, 1340–1346.
- N. Padmanathan, S. Selladurai and K. M. Razeeb, *RSC Adv.*, 2015, **5**, 12700–12709.
- S. Yang, *Science*, 2015, **348**, 396–397.
- A. T. Haedler, K. Kreger, A. Issac, B. Wittmann, M. Kivala, N. Hammer, J. Köhler, H. W. Schmidt and R. Hildner, *Nature*, 2015, **523**, 196–199.
- J. Gao, R. S. Ndong, M. B. Shiflett and N. J. Wagner, *ACS Nano*, 2015, **9**, 3243–3253.
- S. J. Lee, J. M. Baik and M. Moskovits, *Nano Lett.*, 2008, **8**, 3244–3247.
- J. Wang, J. Zhang, A. K. Sundramoorthy, P. Chen and M. B. Chan-Park, *Nanoscale*, 2014, **6**, 4560–4565.
- G. Li, Y. Wang and L. Mao, *RSC Adv.*, 2014, **4**, 53649–53661.
- J. V. Pellegrotti, G. P. Acuna, A. Puchkova, P. Holzmeister, A. Gietl, B. Lalkens, F. D. Stefani and P. Tinnefeld, *Nano Lett.*, 2014, **14**, 2831–2836.
- F. M. Kelly and J. H. Johnston, *ACS Appl. Mater. Interfaces*, 2011, **3**, 1083–1092.
- R. Zhang, W. Lin, K. Moon and C. P. Wong, *ACS Appl. Mater. Interfaces*, 2010, **2**, 2637–2645.
- A. Salehi-Khojin, H. M. Jhong, B. A. Rosen, W. Zhu, S. Ma, P. J. A. Kenis and R. I. Masel, *J. Phys. Chem. C*, 2013, **117**, 1627–1632.
- S. Ghosh, S. Khamarui, M. Saha and S. K. De, *RSC Adv.*, 2015, **5**, 38971–38976.
- S. Anandhakumar, M. Sasidharan, C. W. Tsao and A. M. Raichur, *ACS Appl. Mater. Interfaces*, 2014, **6**, 3275–3281.
- X. H. Zhao, Q. Li, X. M. Ma, Z. Xiong, F. Y. Quan and Y. Z. Xia, *RSC Adv.*, 2015, **5**, 49534–49540.
- F. J. Garcia-Vidal, J. B. Pendry, *Phys. Rev. Lett.*, 1996, **77**, 1163–1166.
- S. Nie, S. R. Emory, *Science*, 1997, **275**, 1102–1106.
- S. Q. Li, P. Guo, D. B. Buchholz, W. Zhou, Y. Hua, T. W. Odom, J. B. Ketterson, L. E. Ocola, K. Sakoda and R. P. H. Chang, *ACS Photonics*, 2014, **1**, 163–172.
- G. C. Schatz, M. A. Young, R. P. V. Duyne, *Top. Appl. Phys.*, 2006, **103**, 19–45.
- K. Xu, J. Huang, Z. Ye, Y. Ying and Y. Li, *Sensors*, 2009, **9**, 5534–5557.

30. X. Zhang, M. A. Young, O. Lyandres and R. P. Van Duyne, *J. Am. Chem. Soc.*, 2005, **127**, 4484–4489.
31. A. Sujith, T. Itoh, H. Abe, K. Yoshida, M. S. Kiran, V. Biju and M. Ishikawa, *Anal. Bioanal. Chem.*, 2009, **394**, 1803–1809.
32. C. W. Chiu, C. C. Chu, W. T. Cheng and J. J. Lin, *Euro. Polym. J.*, 2008, **44**, 628–636.
33. C. W. Chiu, C. C. Chu, S. A. Dai and J. J. Lin, *J. Phys. Chem. C*, 2008, **112**, 17940–17944.
34. Y. Shiraishi, H. Hirakawa, Y. Togawa and T. Hirai, *ACS Catal.*, 2014, **4**, 1642–1649.
35. C. Otto, T. J. J. van den Tweel, F. F. M. de Mul and J. Greve, *J. Raman Spectrosc.*, 1986, **17**, 289–298.
36. A. Li, Z. Baird, S. Bag, D. Sarkar, A. Prabhath, T. Pradeep and R. G. Cooks, *Angew. Chem., Int. Ed.*, 2014, **53**, 12528–12531.
37. X. Zou and S. Dong, *J. Phys. Chem. B*, 2006, **110**, 21545–21550.
38. T. T. B. Quyen, W. N. Su, C. H. Chen, J. Rick, J. Y. Liu and B. J. Hwang, *J. Mater. Chem. B*, 2014, **2**, 5550–5557.